Available online at www.sciencedirect.com
SCIENCE DIRECT®

Journal of the European Ceramic Society 23 (2003) 3089–3096

www.elsevier.com/locate/jeurceramsoc

Young's modulus measurements of magnesia–spinel composites using load–deflection curves, sonic modulus, strain gauges and Rayleigh waves

Cemail Aksel[a,*], Frank L. Riley[b]

[a]*Department of Materials Science and Engineering, Anadolu University, Iki Eylül Campus, Eskisehir 26470, Turkey*
[b]*Department of Materials, School of Process, Environmental and Materials Engineering, University of Leeds, Leeds LS2 9JT, UK*

Received 21 September 2002; received in revised form 16 January 2003; accepted 1 February 2003

Abstract

The extent of interlinking of the microcracking and a decrease in strength and modulus values were determined to be a function of both spinel particle size and volume fraction to allow calculation of thermal shock parameter, R‴. Measurements of Young's modulus were carried out both at room temperature and after thermal shock testing by using the load–deflection curves (defined as "mechanical" modulus) and by the sonic modulus technique. The values obtained from these methods were significantly different for quenched/unquenched samples. To understand the basis for these differences, strain gauge and Rayleigh wave methods were also used to determine Young's modulus of the composites. Modulus values obtained from these methods confirmed the differences measured, and provided a guide to the values to be used in calculating thermal shock parameters. The mechanical modulus technique was considered the most meaningful indicator of Young's modulus for a situation in which large mechanical strains were to be applied to the materials during thermal shock.

Keywords: Mechanical modulus; $MgAl_2O_4$; MgO; Rayleigh waves; Sonic modulus; Strain gauge; Thermal shock

1. Introduction

The elastic properties of ceramics determine mechanical behaviour and are dependent on crystal structure and bonding. Young's modulus decreases as temperature is increased, due to lattice expansion.[1] The effects of porosity on the physical properties of ceramics have also been observed in many studies on sintering and designed in development programme to establish optimum forming and firing procedures for commercial production. However, changes in processing and composition variables usually produce changes in crystal size, pore size and shape. It is therefore difficult to evaluate the effect of porosity alone. The solid phase is continuous with isolated pores. Porosity does not affect the expansion coefficient in isotropic polycrystalline bodies. In bodies composed of anisotropic crystals the effect of porosity is expected to be small. Minimum changes are observed when the solid phase is continuous. The largest changes occur when the pore phase is continuous where only point contact exists between solid grains.[2] When the pores are randomly distributed, the effect of porosity on strength and elastic moduli is smaller.[2]

The reduction in Young's modulus cannot be explained only by the porosity. The decrease in moduli is attributed to the formation of spontaneous microcracking.[3] In terms of elastic strain on a stress–strain curve, the introduction of either pores or pre-existing cracks leads to a reduction in Young's modulus and to an equivalent increase in elastic strain for a given stress. The increase in elastic strain on the basis of the crack-opening displacement is caused by the presence of radial and/or annular cracks associated with the pores.[4] The values of Young's modulus decrease with increasing degree of microcracking, depending on the nature of crack interaction. Heavily microcracked materials exhibit a Young's modulus substantially lower than non-

* Corresponding author. Tel.: +90-222-335-0580x6355; fax: +90-222-323-9501.
E-mail address: caksel@anadolu.edu.tr (C. Aksel).

0955-2219/03/$ - see front matter © 2003 Elsevier Ltd. All rights reserved.
doi:10.1016/S0955-2219(03)00103-1

microcracked materials.[5] For example, MgO has a compact microstructure with a small percentage of discontinuities, which can initiate cracking. MgO–chromite bricks exhibit lower Young's modulus as compared to MgO bricks.[6] For example in the MgO–spinel system, Young's modulus falls to a minimum with increasing spinel content at 30–40% addition.[1,7] However, Young's modulus increases significantly with spinel content >40% (e.g. back to the MgO value). As the spinel becomes the continuous phase, Young's modulus stayed approximately constant between 50 and 80%.[1]

Magnesium aluminate spinel ($MgAl_2O_4$) is an important constituent of MgO-based refractory materials. Spinel particles are added in various proportions to MgO to improve thermal shock resistance.[8–10] Thermal shock only occurs during the heating and cooling periods, when temperature changes can be large and rapid, leading to large thermal stresses.[11] Fired MgO–spinel brick exhibits high resistance to thermo-mechanical stress.[12] The reason for these improvements[13] is linked to the large difference in thermal expansion coefficient between MgO (13.6×10^{-6} °C^{-1} from 25 °C to 1000 °C) and spinel (8.4×10^{-6} °C^{-1} from 25 °C to 1000 °C).[14,15] This difference leads to the development of large tensile stresses, and eventually extensive microcracking, around spinel grains during cooling from fabrication temperatures in excess of 1600 °C.[12,16,17] Due to the microcrack development around the spinel grains, the radial cracks produced readily link together.[16,17] The improved resistance to thermal shock observed in MgO–spinel composites can therefore be attributed to the microcrack networks developed around the spinel particles.[18–20]

There seems to exist a critical volume fraction above which spontaneous microcracking will occur and this critical volume fraction is related to the critical grain size. The reason for the dependence on volume fraction is associated with the residual tensile stresses in the composites. It was found that tensile stresses in the matrix will increase with increasing volume fraction of an additive. Therefore, composites using particles with sizes less than the critical size at a specific volume fraction do not eliminate the formation of spontaneous microcracking at higher volume fractions. Spontaneous microcracking leads to reductions in Young's modulus.[3]

In terms of microcracking, Young's modulus values are important to determine thermal shock resistance. A non-uniform distribution of cracks of random or preferred orientation can also be used to advantage in improving thermal stress resistance.[21] As the microcracking increases, Young's modulus decreases depending on the size of the cracks.[22] As significant amount of microcracks appears after thermal shock because of thermally induced stresses, permanent loss of stiffness and strength occur.[23] It is considered that this behaviour of strength, and Young's modulus in composites was due to the growth and combination of cracks.[24] The effective elastic modulus of a cracked medium depends on crack shape, density and crack preferred orientation. The measured effective elastic properties of the damaged material represent the effect of microcracks.[23]

In this work, fully dense materials have been obtained and thus the influence of porosity on modulus has been neglected, but attention has been given to the relationship between composition and microcracking, which affects Young's modulus significantly. The extent of interlinking of the microcracking has been investigated as functions of spinel particle size and volume fraction, and the reasons for this are examined. The effects of varying the amounts of spinel with different particle sizes on both strength and Young's modulus using various methods were investigated to allow calculation of thermal shock parameter, R'''. The reliability of different methods determining the modulus values has been established on the basis of thermal shock data to allow detailed modelling of the thermal shock behaviour of magnesia-spinel composite materials of compositions and microstructures matching those of less pure refractory materials.

2. Experimental

MgO powder of >98.0% purity ('light': GPR, BDH, Poole, UK) was calcined at 1300 °C for 2 h, to produce a powder with a mean particle size of 0.5 μm. A >97% dense materials were prepared by hot-pressing at 1700 °C and 20 MPa for 25 min. 12 and 24 μm spinel powders were obtained by crushing and sieving high density (~98% purity) spinel 'pebbles' (Britmag 67, Redland Minerals, UK). The stoichiometry of spinel by weight% is given as follows: 66.3% Al_2O_3, 31.6% MgO and 2.1% the total amounts of impurities. MgO containing spinel particles reached the theoretical density (~99%), by hot-pressing at 1720 °C and 20 MPa for 25 min. Samples for measuring Young's modulus with flat, parallel ends were required. The ends of these samples were cut parallel to each other using a diamond cutter (Struers Accutom-2), which allowed precise alignment of the samples and performed precision cutting. Young's modulus values of MgO and MgO–spinel composites were measured, as a function of particle size and spinel addition at room temperature using various techniques (Sections 2.1–2.4). The R''' parameter, expressing the ability of a material to resist crack propagation and further damage on thermal shocking, was calculated by the formula, $\{R''' = E/[\sigma_f^2\cdot(1-\nu)]\}$,[25–27] where E is Young's modulus, σ is strength, and ν is Poisson's ratio. Thermal-shock tests were then made by holding the rectangular specimens for at least 20 min to allow for temperature equilibration in a vertical tube furnace maintained at 1000 °C and dropping them into a container of silicone oil at room temperature, which

was being stirred with a magnetic stirrer (at room temperature). After cleaning with acetone, samples were dried in an oven at 110 °C before breaking in three-point bend. Young's moduli of composites and pure MgO were measured after quenching from 200 to 1000 °C, at 200 °C intervals, using load–deflection curves (mechanical modulus-E_m) and the sonic modulus (E_s) techniques, as a function of quench temperature. Thermal shock results were then evaluated on the basis of the calculated R''' parameter. The CamScan 4 SEM equipped with an EDX system for elemental analysis was also used to examine the size, shape, texture of the particles, the presence and position of second phases in the polished surface of the multiphase materials.

2.1. Modulus from stress–strain data

Modulus measurements were made at room temperature and after thermal shock testing in three-point bend, using bars of dimension of $26\times3\times2.5$ mm^3. Five specimens were normally used to obtain each mean value, with a support roller span of 20 mm and a cross-head speed of 0.2 mm min^{-1}. Mechanical modulus (E_m) values were calculated by drawing a tangent to the steepest initial straight-line portion of the load–deflection curve, where the stiffness of the machine was also considered, using Eq. (1)[28]

$$E_m = L^3 m/\left(4WD^3\right) \quad (1)$$

where L = support span, W = width of bar, D = depth of bar, and m = slope of the tangent of the initial straight-line portion of the load–deflection curve.

2.2. Sonic modulus

A sonic modulus method was also used to measure Young's modulus. This is a procedure for measuring the resonance frequency, based on the vibration of a rectangularly shaped specimen at room temperature.[29] The test required the samples to be electrically conductive, and samples were painted on both their ends with silver paint, and a thin stripe along their length. The sample was clamped at its middle point by two knife edge supports on the testing apparatus, electrically earthed, and placed between two electrodes with a voltage of ~200 V. The electrodes were brought very close to the specimen ends (usually <0.2 mm) to form parallel-plate capacitors with the flat ends of the specimen. In addition, a small periodic voltage of the order of a few mV was fed to one of the electrodes, the driver electrode, which set the sample into vibration caused by the oscillating electrostatic field. The parallel-plate capacitor on the other end sensed the oscillation by means of changing charges due to changing capacitance caused by the vibration. Test specimens were vibrated in a broad frequency range: the electrode was used to sense the resulting mechanical vibrations of the specimen and transform them into an electrical signal that could be displayed on the screen of an oscilloscope used to detect fundamental and harmonic vibration frequencies.[29] Longitudinal vibration occurs by a sinusoidal force applied to one of the parallel ends. The stress wave propagates down the specimen and is reflected at the other end. The frequency of vibration of the specimen was recorded that resulted in a maximum displacement, having a well-defined peak on the indicator.[30] The standard equation [29,30] for the sonic modulus (E_S) is:

$$E_S = 4.f^2.l^2.\rho \quad (2)$$

where: f = frequency of longitudinal mode of vibration (velocity of sound/wavelength), l = length of the specimen, and ρ = density of the specimen. Specimens having either very small or very large ratios of length to thickness may be difficult to excite in the fundamental modes of vibration. To apply this method, the ratio must be between 5 and 20.[30] This method is non-destructive, and specimens used for this method can subsequently be used for other tests.

2.3. Strain gauges

In order to compare and confirm the results obtained from the mechanical and sonic modulus methods, specimens were also loaded with a strain gauge in the central zone between the inner loading rollers on the tensile faces, using a support roller span of 20 mm, and a cross-head speed of 0.2 mm min^{-1}. Measurements were made using the four-point bend test.[31] The equations developed[32,33] for the measurement of strain (ϵ), resistance ($\Re$), and output voltage data (ϵ_d) are:

$$\epsilon = 100[(\Re - r)/(k_{SG}.\Re)] \quad (3)$$

$$\Re = \left\{[r(\epsilon_d/G) + 300]/[\mathrm{Vo} - \epsilon_d/G]\right\} \quad (4)$$

where:

r = (resistance of amplifier plus nominal resistance of strain gauge at 21 °C(120 Ω))

ϵ_d = Output voltage (plus 5.10^6 to make positive the all data)

G = Amplifier gain setting/10^8

Vo = Half bridge voltage across Wheatstone Bridge (2.5 V)

k_{SG} = Strain gauge constant (2.14).

2.4. Rayleigh waves

To measure the Rayleigh wave velocity in the line-focus acoustic microscope a ZnO transducer is used to launch an acoustic wave along a sapphire lens. Water acts as a couplant to transmit the acoustic energy from the lens to specimen. At the sapphire/water interface

waves are refracted towards the sample. Two waves are of interest: one travels straight down to the specimen and is reflected back along the axis of the lens. The second wave is refracted at the Rayleigh angle, θ_R, typically about 30°. This wave excites a leaky Rayleigh wave in the surface of the specimen, which in turn radiates a wave back towards the lens. The net signal received at the transducer is the phase-sensitive sum of these two waves. As the specimen is scanned up towards the lens (z-scan) the voltage output, $V(z)$, shows oscillations, the period of which, Δz, is related to the velocity of the Rayleigh wave, v_R, by the following equation:[34,35]

$$V_R = \frac{V_w}{\left[1-(1-V_w/2f\Delta z)^2\right]^{1/2}} \quad (5)$$

where v_w is the velocity of sound in water ($\sim$1500 m s^{-1} at room temperature) and f is the frequency of the sound generated. In the microscope used in this work, f = 225 MHz. The shear velocity, v_s is:

$$v_s = v_R/\left(1.14418 - 0.25771\nu + 0.12661\nu^2\right) \quad (6)$$

where v_R is the Rayleigh wave velocity and ν Poisson's ratio. Given the Rayleigh wave velocity, Poisson's ratio (ν: 0.29) and density (ρ: 3.52 Mg m^{-3}); elastic modulus E was calculated from the equation as follow:

$$E = 2G(1+\nu) = 2\rho v_s^2(1+\nu) \quad (7)$$

3. Results and discussion

3.1. Strength and Young's modulus

As shown in Table 1, the room temperature strength of the hot-pressed pure MgO was in good agreement with the literature values of $\sim$225 and 230 MPa[36,37] for $\sim$32 and 25 μm MgO grain sizes, respectively. The addition of up to 10% of the spinel powder to MgO decreased the strength significantly ($\sim$75%). Further additions caused no further loss (though they may have been a slight increase at 30% addition, but the scatter of data was larger). The decrease in strength was greater the coarser the spinel particle size. Spinel content, but predominantly spinel particle size, significantly affected the strength. There was a significantly greater decrease in strength for 24 μm compared to 12 μm spinel particles, and the 24 μm spinel particles were associated with formation of longer cracks than the 12 μm particles (Figs. 1 and 2). The total extent of cracking also increased with increasing concentration of spinel (Fig. 3).

Table 1
Bend strength as a function of spinel content and particle size

Spinel (wt.%)	σ (MPa)				
	0	5	10	20	30
12 μm spinel	233±7	142±17	94±24	62±28	103±22
24 μm spinel	233±7	91±14	48±17	50±10	70±23

The Young's modulus of the pure hot-pressed MgO at room temperature was in good agreement with literature values of $\sim$290 GPa[36] ($\sim$25 μm grain size), and 258 GPa[38] ($\sim$7 μm grain size). The Young's modulus of spinel composites generally decreased with increasing spinel content (Fig. 4). There was little difference between the 12 and 24 μm spinel composites. The decrease in mechanical Young's modulus was most significant, for up to 10% additions. At 10%, Young's modulus was approximately 50% of the value for pure MgO. Increasing the amount of spinel from 10 to 30%,

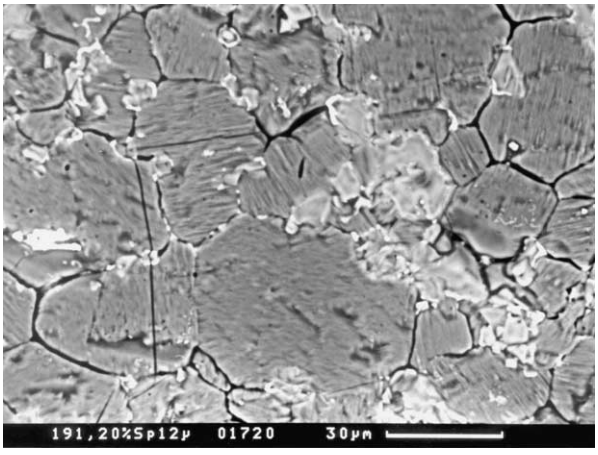

Fig. 1. SEM micrograph of a 20% 12 μm spinel composite (dark grey: MgO, light grey: spinel).

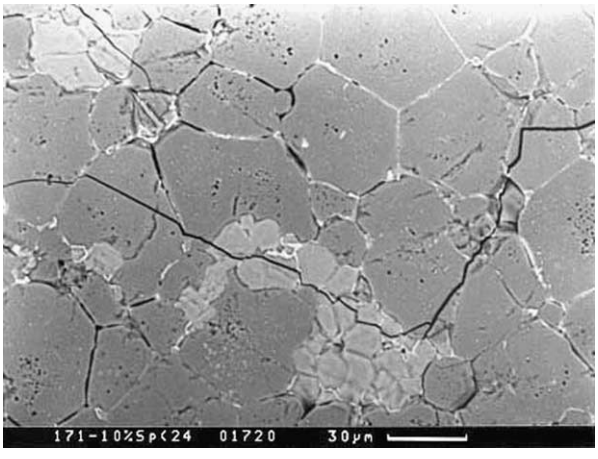

Fig. 2. SEM micrograph of a 10% 24 μm spinel composite (dark grey: MgO, light grey: spinel).

had a relatively small effect. The loss of modulus can be explained in terms of radial crack propagation and ultimately interlinking (Figs. 1–3). It appears that crack interlinking is completed at about 10% addition of spinel, undermining the mechanical integrity of the material, and changes little after this point. In contrast, Young's modulus values determined by the sonic method were approximately twice the mechanical modulus values for spinel amounts $\geqslant 10\%$, and showed a smaller decrease with increasing spinel content.

The modulus values determined using strain gauges for pure MgO were in reasonable agreement with the sonic modulus and mechanical modulus values. There is thus consistency, within the limits of experimental errors, between these data. On the other hand, Young's modulus for pure MgO calculated using Rayleigh waves was less than the calculated from the stress–strain curve (7%), and the value measured using the sonic modulus technique (12%).

Young's modulus values calculated using Rayleigh waves were close to values measured using the sonic modulus technique, and the values obtained using strain gauges were also close to the values from the stress–strain measurements. For this reason, mechanical modulus and sonic modulus methods were used for both unquenched and quenched samples, containing spinel powders, because significantly different values were obtained from each method, the origin of which needed to be investigated.

Mechanical Young's moduli of composites decreased with additions of spinel, for each particle size (Fig. 1). SEM observations showed that (in Figs. 1–3) coarse particles were associated with longer crack formation, compared to fine particles. The crack lengths also increased with increasing concentration of spinel.

The decrease in mechanical modulus was significantly greater, the higher the spinel content. The changes in sonic modulus values followed a similar pattern to the mechanical modulus. However, sonic modulus values for spinel composites, showed only small changes with increasing spinel content, compared to pure MgO. Fig. 4 showed that when the spinel content of composites increased, both values decreased, but the mechanical modulus showed a more marked loss of Young's modulus than the sonic modulus.

3.2. R‴ parameter

Because of the importance of the strength and Young's modulus (E/σ^2) ratios for calculation of thermal shock parameter (R'''), it was of interest to investigate how strength and Young's modulus varied for each composition. The R''' parameter[25–27] gives information about available energy at fracture for resisting to crack propagation, and high values indicate an improvement in thermal shock resistance.

The variations of R''' parameter for MgO and spinel composites are shown in Fig. 5. On the basis of mechanical modulus (E_m) and sonic modulus (E_s) data, 24 μm spinel composites attained by far the highest R''' parameter values. For the 24 μm spinel, the maximum R''' value was at 10% addition; the 12 μm spinel B had a maximum at ~20%. The maximum R''' parameters for the 12 and 24 μm spinel composites were approximately 7–12 times (using E_m) and 11–21 times (using E_s) larger,

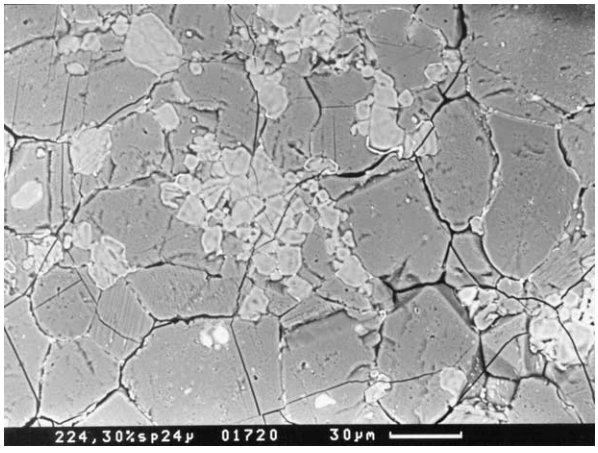

Fig. 3. SEM micrograph of a 30% 24 μm spinel composite (dark grey: MgO, light grey: spinel).

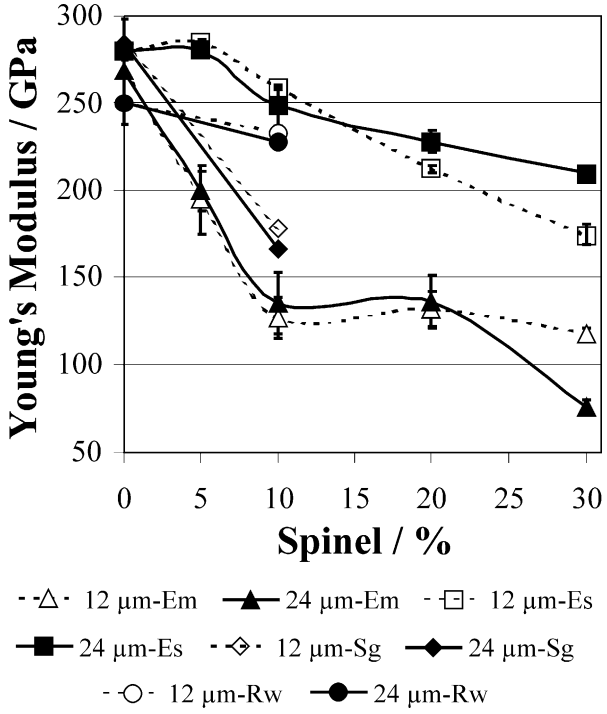

Fig. 4. Young's modulus of MgO and MgO–spinel composites as a function of spinel content and particle size: mechanical modulus (E_m), sonic modulus (E_s), strain gauges (S_g), and Rayleigh waves (R_w).

respectively, than that of pure MgO (Fig. 5). These trends indicate that strength values were initially more sensitive to composition than Young's modulus, but as modulus values decreased slightly with increasing additions, strength remained approximately constant (Fig. 4 and Table 1). It is seen that the effect of incorporating spinel into magnesia is to cause a sharp decrease in strength, through microcrack generation. The strength and Young's modulus values decreased with spinel additions, and the influence of the spinel was observed to be more marked the larger the spinel particle size. Strengths of the coarser spinel composites were in general much more sensitive to composition than was Young's modulus, noting the wide spread of particle sizes. R''' parameter shows that the smaller the spinel particle size, the lower the resistance to crack propagation (Fig. 5). Materials containing 12 μm spinel had short length cracks originating from the spinel particles; the 24 μm spinel particles were the origin of longer cracks, and more crack initiation sites (Figs. 1–3). On the basis of the calculated R''' values, coarse spinel particles are generally more beneficial than the fine particles, for which a very much larger volume appears to be required to achieve the same improvement. As shown in Fig. 5, the thermal shock resistance of 10% 24 μm spinel composites was predicted to be ~2 times greater than those obtained from 20% 12 μm spinel composites. It was therefore expected that resistance to crack propagation in general would be greater with materials containing the coarsest spinel particle size.

3.3. Thermal shock testing

The Young's moduli of pure MgO and spinel composites, were also measured after shock from temperatures at 200 °C intervals up to 1000 °C (Fig. 6). For each material the Young's modulus decreased gradually with increasing shock temperature up to ~575 °C. After quenching between 575 and 625 °C, the Young's modulus of MgO fell to about 30% of the initial value, because of the nucleation of microcracks and their propagation. Above 625 °C, Young's modulus decreased more slowly with increasing temperature (Fig. 6), presumably because the number of cracks increased only slightly with increase in the thermal shock temperature. In contrast, spinel composites tested showed a stable trend (Fig. 6). The cracks initiated by thermal shock seemed to propagate only a short distance and were then arrested rather than that the cracks had a sudden extension, giving catastrophic fracture. For this reason, there was a gradual decrease in the Young's modulus of composites.

Fig. 6 shows that the mechanical Young's modulus of pure MgO decreased abruptly in the temperature range 575–625 °C. Above this temperature, mechanical modulus decreased gradually with increasing shock temperature. In contrast, there was in general a slight decrease in sonic modulus values of MgO with increasing shock temperature. Even when the crack length increased and more cracks were introduced by thermal shocking, the sonic technique was unable to detect the microcracks. A similar, but more stable trend, was also observed for the spinel composites by using both methods: there was a marked decline in mechanical modulus values whereas sonic modulus values remained almost at the same level, with increasing quench temperature.

On the basis of the prediction from the R''' parameter values; sonic modulus data seemed to illustrate the highest resistance to crack propagation, for 10% 24 μm spinel composites, in comparison with the values obtained from mechanical modulus (Fig. 5). However, thermal shock results showed that sonic modulus values of MgO were still higher than that of spinel composites. On the other hand, mechanical modulus values of spinel composites was much higher than pure MgO at the highest quench temperature used, even more cracks

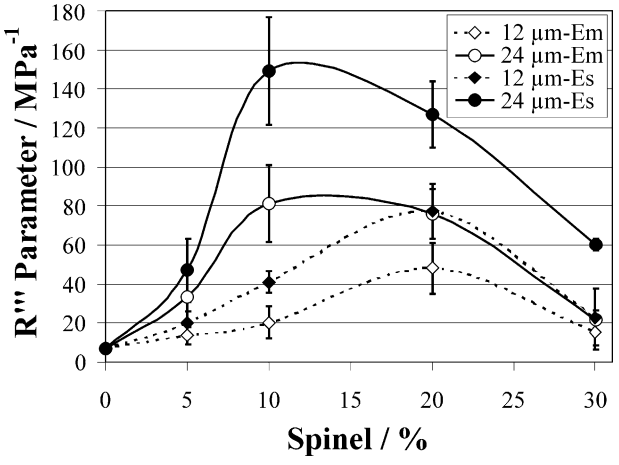

Fig. 5. R''' parameter as a function of spinel content and particle size: mechanical modulus (E_m) and sonic modulus (E_s).

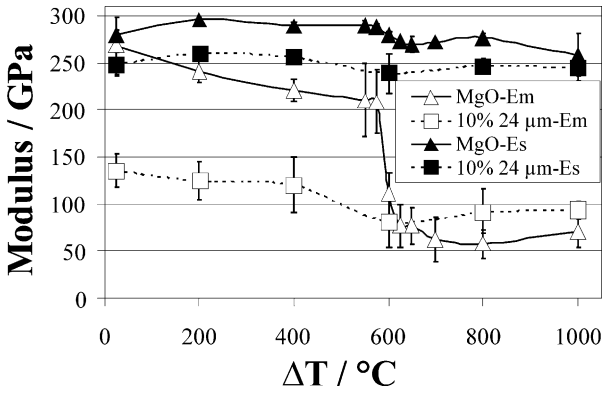

Fig. 6. Mechanical modulus from load–deflection curve (E_m) and sonic modulus (E_s), as a function of quench temperature.

were introduced by thermal shocking (Fig. 6). R''' parameter values obtained from mechanical modulus method are thus in good agreement with the thermal shock test data. For this reason, mechanical modulus, E_m, was found to be the most reliable indicator for evaluating Young's modulus data rather than using sonic modulus technique for those materials.

These results suggest that this behaviour of Young's modulus was because of the formation and interlinking of microcracks, which is most marked for MgO, in comparison with the spinel composites. Spinel composites were not as badly cracked, as in the MgO materials, and a high concentration of larger cracks was not occurred at the critical quench temperature of MgO. A gradual decrease in the Young's modulus occurred because of the high levels of pre-formed thermal expansion mismatch microcracks already present in the structure. With increase in microcrack density after thermal shock, crack interaction effects became more important. The high thermal shock resistance was attributed to the interlinking of high level of pre-existing microcracking occurred in the spinel materials.

3.4. Comparison of Young's modulus measurements

Young's modulus values obtained for spinel composites using strain gauges were very close (e.g. with an ~5% deviation) to the values from the stress–strain mechanical measurements, and the values obtained using Rayleigh waves were quite close (e.g. in the range of ~10%) to the values measured using the sonic modulus technique (Fig. 4). Mechanical modulus and sonic modulus methods used in this work gave significantly different values. It is suggested that when a material has a higher expansion coefficient than the second phase particles it contains, then during cooling, the matrix will clamp down onto the second phase. It is clear that in the case of the MgO–spinel composites, this results in the production of very narrow radial microcracks (Figs. 1–3), because of the hoop stress developed around the spinel particles. These materials then provide a continuous mechanical path through the MgO matrix for the sound pulse to follow. In contrast, wider microcracks occurring in more severely shocked materials disrupt the sound pulse, and must then be no direct solid path: a lower sonic modulus value is seen, because of a decrease in the velocity of the sound wave, and hence resonance frequency. However, there was in general a slight decrease in sonic modulus values with even increasing shock temperature (Fig. 6). The mechanical modulus would clearly be influenced by the matrix microcracking to a much greater extent. Interpretation of the sonic modus data is not straightforward. It appears that in materials which contain relatively small amounts of local microcracking arising from the thermal expansion mismatch (the composites), or from milder thermal shocking (in MgO for example) the sound wave does not really detect the presence of the cracks. This is because the crack is insufficiently wide to prevent bridging by the crack front. In the case of very severely shocked materials a decrease in the sonic modulus values starts to be seen (Fig. 6), and the greater crack width, or density now appears to have an influence on the sound wave. The key criteria may be whether the cracks are sufficiently wide, or have propagated to form a continuous link amongst the spinel particles. The above observations explain that the sonic modulus technique is not a sensitive detector of certain types of flaw generated in these materials, and gives consistently higher values than the mechanical modulus technique. It was therefore decided that the evaluation of thermal shock parameters should be more reliable on mechanical Young's modulus measurements, calculated from load deflection curves. This also applied to quenched samples, for which even lower mechanical modulus values were obtained.

4. Conclusions

It is suggested that Rayleigh waves and the sonic modulus technique cannot detect fine microcracks, and it cannot therefore give reliable information about cracked materials. Even when more cracks were introduced by quenching from above the critical quench temperature for MgO, the sonic technique could not provide a sensitive detector of microcracking. Furthermore, the load applied during the sonic modulus measurements to specimens was insignificant, and further extended microcracking would not have been caused. The mechanical modulus technique (using the load–deflection curves) was considered the most meaningful indicator of Young's modulus in the evaluation of thermal shock parameters for a situation in which large mechanical strains were to be applied to materials by thermal shock. This is also supported by the R''' parameter values and confirmed by the thermal shock test data. In addition, Young's modulus values of spinel composites in general decreased with increasing spinel content. Modulus appeared to be more sensitive to spinel content than to spinel particle size.

Acknowledgements

Redland Minerals (UK) is thanked for supplies of materials. The contributions of Dr. P.D. Warren, Prof. B. Rand and the late Prof. R.W. Davidge are gratefully acknowledged. Special thanks go to Dr. C. Lawrence for his help with Rayleigh Wave method. The authors also wish to thank Dr. Roger Morrell, whose invaluable expertise in this field was greatly appreciated. Dr. P.

Bartha, Dr. S. Plint, and M.W. Roberts are also thanked for helpful discussions. This work was in part carried out as part of a PhD programme in the Department of Materials of the University of Leeds, and the authors thank the Technical Staff of the Department for their assistance. Financial support was provided in part by the Council of Higher Education in Turkey.

References

1. Cooper, S. C. and Hodson, P. T. A., Magnesia–magnesium aluminate spinel as a refractory. *Trans. J. Brit. Ceram. Soc.*, 1982, **81**, 121–128.
2. Coble, R. L. and Kingery, W. D., Effect of porosity on physical properties of sintered alumina. *J. Am. Ceram. Soc.*, 1956, **39**, 377–385.
3. Chou, Y. S. and Green, D. J., Silicon carbide platelet/alumina composites: II, mechanical properties. *J. Am. Ceram. Soc.*, 1993, **76**, 1452–1458.
4. Krstic, V. D. and Ericson, W. H., A model for the porosity dependence of Young's modulus in brittle solids based on crack opening displacement. *J. Mater. Sci.*, 1987, **22**, 2881–2886.
5. Hasselman, D. P. H., Thermal stress resistance parameters for brittle refractory ceramics: a compendium. *Am. Ceram. Soc. Bull.*, 1970, **49**, 1033–1037.
6. Szmeja, B. T. and Wala, T. B., Thermal shock acoustic emission and microstructure of refractories II. Basic refractories. *Ceram. Int.*, 1994, **20**, 367–377.
7. Aksel, C., *Thermal Shock Behaviour and Mechanical Properties of Magnesia–Spinel Composites*. PhD Thesis, Department of Materials Engineering, University of Leeds, Leeds, UK, 1998.
8. Bartha, P., Magnesia spinel bricks—properties, production and use. In *Proc. Int. Symp. Refractories, Refractory Raw Materials and High Performance Refractory Products*, ed. X. Zhong et al. Pergamon, Hangzhou, 1989, pp. 661–674.
9. Klischat, H. J. and Bartha, P., Further development of magnesia spinel bricks with their own specific properties for lining the transition and sintering zones of rotary cement kilns. *World Cement,* 1992, 52–58.
10. Kimura, M., Yasuda, Y. and Nishio, H., Development of magnesia spinel bricks for rotary cement kilns in Japan. In *Proc. 26th Int. Col. Ref.*, Interceram Special Issue, 1984, Vol. 33, Aachen, Germany, 1983 pp. 344–376.
11. Geisler, T. A., Finite element analysis of thermal stresses in cement kiln brick. In *UNITECR '89*, Anaheim, USA, 1989, pp. 1317–1327.
12. Soady, J. S., and Plint, S., A quantitative thermal shock approach to the development of magnesia-spinel refractories for the cement kiln. In *UNITECR '91*, Aachen, Germany, 1991, pp. 443–449.
13. Tabbert, W. and Klischat, H. J., Magnesia spinel bricks for the cement industry. In *Proceedings Beijing China Symposium*, China, 1992, pp. 424–430.
14. Shackelford, J. F., Alexander, W. and Park, J. S., (eds), *CRC Materials Science and Engineering Handbook*. CRC Press, Boca Raton, FL, 1994.
15. Burnett, S. J., *Properties of Refractory Materials*. UKAEA Research Group Report, Harwell, 1969.
16. Aksel, C., Davidge, R. W., Warren, P. D. and Riley, F. L., Mechanical properties of model magnesia–spinel composite materials. In *Euro Ceramics V, Part 3, Extended Abstracts of the 5th Conference and Exhibition of the European Ceramic Society*, *Key Engineering Materials*, Vols 132–136, Versailles, France, 1997, pp. 1774–1777.
17. Aksel, C., Davidge, R. W., Knott, P. and Riley, F. L., Mechanical properties of magnesia–magnesium aluminate spinel composites. In *III. Ceramic Congress Proceedings Book, Engineering Ceramics*, Vol. 2, Istanbul, Turkey, 1996, pp. 172–179.
18. Aksel, C., Rand, B., Riley, F. L. and Warren, P. D., Mechanical properties of magnesia–spinel composites. *J. Eur. Ceram. Soc.*, 2002, **22**, 745–754.
19. Aksel, C. and Warren, P. D., Thermal shock parameters [R, R''' and R''''] of magnesia-spinel composites. *J. Eur. Ceram. Soc.*, 2003, **23**, 301–308.
20. Aksel, C., Davidge, R. W., Warren, P. D. and Riley, F. L., Investigation of thermal shock resistance in model magnesia–spinel refractory materials. In *IV. Ceramic Congress, Proceedings Book, Part 1*, Eskisehir, Turkey, 1998, pp. 193–199.
21. Kingery, W. D., Factors affecting thermal stress resistance of ceramic materials. *J. Am. Ceram. Soc.*, 1955, **38**, 3–15.
22. Hasselman, D. P. H. and Singh, J. P., Analysis of thermal stress resistance of microcracked brittle ceramics. *Am. Ceram. Soc. Bull.*, 1979, **58**, 856–860.
23. Rokhlin, S. I., Chu, Y. C. and Baaklini, G. Y., Assessment of damage in ceramics and ceramic matrix composites using ultrasonic techniques. *Journal of Engineering for Gas Turbines and Power*, 1995, **117**, 417–423.
24. Matsuuhita, K., Kuratani, S., Okamoto, T. and Shimada, M., Young's modulus and internal friction in alumina subjected to thermal shock. *J. Mater. Sci. Lett.*, 1984, **3**, 345–348.
25. Hasselman, D. P. H., Elastic energy at fracture and surface energy as design criteria for thermal shock. *J. Am. Ceram. Soc.*, 1963, **46**, 535–540.
26. Hasselman, D. P. H., Unified theory of thermal shock fracture initiation and crack propagation in brittle ceramics. *J. Am. Ceram. Soc.*, 1969, **52**, 600–604.
27. Sack, R. A., Extension of Griffith's theory of rupture to three dimensions. *Proc. Physical Soc., London*, 1946, **58**, 729–736.
28. ASTM D790M-86, *Standard Test Methods for Flexural Properties of Unreinforced and Reinforced Plastics and Electrical Insulating Materials*, *Annual Book of ASTM Standards*, Vol. 08.01. ASTM, 1988, pp. 290–298.
29. ASTM C885-881, *Standard Test Method for Young's Modulus of Refractory Shapes by Sonic Resonance*, *Annual Book of ASTM Standards*, Vol. 17. ASTM, 1982, pp. 964–970.
30. ASTM C747-774, *Standard Test Method for Moduli of elasticity and fundamental frequencies of carbon and graphite materials by sonic resonance*, *Annual Book of ASTM Standards*, Vol. 17. ASTM, 1982, pp. 764–774.
31. ASTM C1161-90, *Standard Test Method for Flexural Strength of Advanced Ceramics at Ambient Temperature*, *Annual Book of ASTM Standards*, Vol. 15.01. ASTM, 1991, pp. 327–333.
32. *Strain Gauges Catalogue*. TML Pam E-101I, Tokyo Sokki Kenkyujo Co., Ltd., 8-2, Minami-ohi 6-chome, Shinagawa-Ku, Tokyo 140-8560, Japan.
33. Marshall, C. W. and Maringer, R. E., *Dimensional Instability—An Introduction*. Pergamon Press, Battelle, Columbus Laboratories, Columbus, OH, USA, 1977.
34. Rayleigh, L., On waves propagated along the plane surface of an elastic solid. *Proc. Lond. Math. Soc.*, 1885, **17**, 4–11.
35. Briggs, G. A. D., *Acoustic Microscopy*. Oxford University Press, Oxford, 1992.
36. Davidge, R. W., *Mechanical Behaviour of Ceramics*. Cambridge University Press, Cambridge, 1979.
37. Rice, R. W., Strength and fracture of hot-pressed MgO. *Proc. Brit. Ceram. Soc.*, 1972, **20**, 329–363.
38. Llorca, J. and Ogawa, T., Crack wake effects on MgO fracture resistance. In *Fracture Mechanics of Ceramics*, Vol. 9, eds. R. C., Bradt, D. P. H., Hasselman, D., Munz, M. Sakai, V. Ya., Shevchenko. 1992, pp. 305–317.